Simultaneous Measurement of Vibrations on Arterial Wall Upstream and Downstream of Arteriostenosis Lesion and Their Analysis

Kazuhiro SUNAGAWA[1,2], Hiroshi KANAI[1], EJSUM, Yoshiro KOIWA[3], Keiko NITTA[4], SJSUM, and Motonao TANAKA[4], SJSUM

Abstract

Acute myocardial infarction and cerebral infarction are generally known to be caused primarily by the rupture of atherosclerotic plaques. It is thus necessary for clinical treatment to predict the rupture of these plaques. Blood-flow velocity around atherosclerotic plaques increases as the arteriostenosis lesion progresses, resulting in turbulence downstream of the lesion. The resulting change in blood pressure produces shear stress, and change in this stress affects the rupture of the atherosclerotic plaques. Cerebral ischemic paroxysm and cerebral infarction have been reported to occur in a high percentage of cases in which inner vessel diameter has decreased to less than 70% of its original diameter as a result of stenosis. This explains the use of standard ultrasonic diagnostic equipment to measure blood flow in the screening of the carotid arteries. On the other hand, the noise signal radiated from an aneurysm as a result of blood flow has been measured using the bruit sensor used to diagnose cerebrovascular diseases. Many unsolved problems with regard to the relationship between noise and turbulence in blood flow remain, however. Here, small vibrations on the arterial wall were measured transcutaneously and analyzed both upstream and downstream of the atherosclerotic plaque of a human carotid artery. Characteristics of the resultant vibrations upstream of the stenosis clearly differed from those downstream of it. These results should prove useful in predicting the rupture of atherosclerotic plaques.

J Med Ultrasonics 2001 ; 28 (Winter) : 157-173.

Keywords

atherosclerosis, arteriostenosis, blood flow, small vibration on arterial wall, ultrasound

1. Introduction

The rupture of atherosclerotic plaques is known to cause circulatory diseases like myocardial and cerebral infarction[1)]. The clinician must be able to predict rupture or likelihood of rupture of these plaques. Therefore, our research group proposed a method[2)] for evaluating the elastic properties of the arterial wall by detecting velocity of vibrations on the arterial wall using ultrasonic diagnostic equipment to evaluate atherosclerotic plaques. Increase in velocity of blood flow around stenotic changes in artery resulting from these plaques causes downstream turbulence. The resulting change in blood circulation is thought to affect blood pressure and shear stress that can lead to rupture of the plaques[3)]. Some years ago the hot-film flowmeter was used to detect turbulent blood flow through stenotic areas[4)] ; today, however, turbulent blood flow is easily detected using the FFT Doppler or color Doppler method with ultrasonic diagnostic equipment. Cerebral ischemic paroxysm and cerebral infarction have been reported to occur in a high proportion of cases in which stenosis has reduced the

[1]Department of Electronic Engineering, Tohoku University Graduate School of Engineering, Aramaki-aza-Aoba 05, Aoba-ku, Sendai 980-8579, Japan, [2]Matsushita Communication Sendai R&D Labs. Co., Ltd., Akedori 2-5, Izumi-ku, Sendai 981-3206, Japan, [3]First Department of Internal Medicine, Tohoku University Graduate School of Medicine, Seiryo-cyo 1-1, Aoba-ku, Sendai 980-8574, Japan, [4]Tohoku Welfare Pension Hospital, Fukumuro-aza-Takasago 10, Miyagino-ku, Sendai 983-0005, Japan
Original article is cited in Med Ultrasonics 2000 ; 27(1) : 15-31.

inner diameter of a vessel to less than 70% of its original diameter[5]. Carotid artery screening now uses ultrasound (US) imaging to determine blood flow velocity at stenotic sites of the arteries, and waveform is used to determine stenotic rate, confirm occlusion of the carotid artery or other stenotic lesions, and distinguish between occlusion and stenosis[6].

Acoustic analysis has been used in the attempt to detect blood-flow murmur using a blood-flow sound sensor and to diagnose arterial lesions[7][8]. Vibration of the arterial wall was not detected directly, however, and much remains to be learned about the effects of turbulence on arterial wall vibration.

We therefore measured the wall vibration produced at an artificially induced stenotic site in a silicone rubber tube and in the carotid artery of an arteriosclerotic patient using a phased tracking method[9]. This allowed us to measure vibrations on the arterial wall with US and to evaluate the effects of blood flow on arterial wall vibration at the stenotic site. Results obtained from this study provide useful clues for predicting possible rupture of plaques.

2. Principles of arterial wall vibrations and in vivo measurement system.

2.1 Principles of measuring the velocity of arterial wall vibrations

Phase delay, which varies with total distance that the US pulse travels in the body, occurs as the transmitted US signal returns to the US probe after being reflected by the arterial wall. When US pulses with an angular frequency of $\omega_0=2\pi f_0$ are repeatedly transmitted to the arterial wall at time intervals of ΔT, the phase $\theta(x_i; t)$ of the pulses reflected from the target i are described by the following equation, in which with the sound velocity is c_0, one-way transmission time is $\tau_i(t)$, and distance to the reflecting object is $x_i(t)$.

$$\theta(x_i; t) = 2\omega_0\tau(t) = 2\omega_0\frac{x_i(t)}{c_0} \qquad (1)$$

The phase difference $\Delta\theta(x_i; t+\Delta T)$ between two detected waves $y(x_i; t)$ and $y(x_i; t+\Delta T)$ in the interval of ΔT can thus be obtained from the following equation.

$$\begin{aligned}\Delta\theta(x_i; t+\Delta T) &= \theta(x_i; t+\Delta T)-\theta(x_i; t)\\ &= \frac{2\omega_0}{c_0}\Delta x_i(t+\Delta T) \qquad (2)\end{aligned}$$

In this equation, $\Delta x_i(t+\Delta T)$ is the distance that the object moves is the interval ΔT, and can be expressed as follows.

$$\begin{aligned}\Delta x_i(t+\Delta T) &= x_i(t+\Delta T)-x_i(t)\\ &= \frac{c_0}{2\omega_0}\Delta\theta(x_i; t+\Delta T) \qquad (3)\end{aligned}$$

This $\Delta x_i(t+\Delta T)$ is divided by ΔT to obtain the average velocity $\hat{v}_i(t+\Delta T/2)$ in the interval ΔT.

$$\begin{aligned}\hat{v}_i\left(t+\frac{\Delta T}{2}\right) &= \frac{\Delta x_i(t+\Delta T)}{\Delta T}\\ &= \frac{c_0}{2\omega_0}\frac{\Delta\theta(x_i; t+\Delta T)}{\Delta T} \qquad (4)\end{aligned}$$

In the present study, received reflected waves were detected by quadrature modulation, separated into real $z_{re}(x_i; t)$ and imaginary signals $z_{im}(x_i; t)$, and digitized. The phase $\theta(x_i; t)$ of detected wave at the time when the reflected waves were detected can be obtained from the following equation.

$$\theta(x_i; t) = \tan^{-1}\left(\frac{z_{im}(x_i; t)}{z_{re}(x_i; t)}\right) \qquad (5)$$

US pulses were transmitted almost simultaneously in N directions on the arterial wall to measure vibration at an arteriosclerotic lesion, and upstream and downstream sites[10]. When measuring simultaneously in N directions, pulse repetition frequency is $1/N$th of that when measured in a single direction. Velocity of the vibrations $v_i(t)$ in this case is obtained with the following equation.

$$\hat{v}_i\left(t+\frac{N\cdot\Delta T}{2}\right) = \frac{c_0}{2\omega_0}\frac{\theta(x_i; t+N\cdot\Delta T)-\theta(x_i; t)}{N\cdot\Delta T} \qquad (6)$$

2.2 Determining the velocity of vibrations on the arterial wall using a phased tracking method

During the US examination, the distance between the transducer and the artery changed several hundred micrometers, varying with dilation of the artery. These arterial changes included 100 to 200 μm of simultaneous movement of the anterior and posterior wall. Simultaneous movements were also measured using the M-mode of the conventional US systems. Because of cardiac contraction, however, it was impossible to accurately measure changes in the inner diameter of the artery. Instead, we used the phased tracking method[9], which allowed us to measure with high precision the vibration velocity $v_i(t)$ on the arterial wall that was included in simultaneous movements, by accurate tracking of instantaneous values $x_i(t)$ of position from the surface of the body. Accurate measurement of phase difference $\Delta\theta(x_i; t)$ in ΔT intervals was important. We therefore determined the instantaneous position $x_i(t)$ of the object using the constraint least-squared approach[9].

The position $x_i(t+\Delta T)$ of the object i at a given time $t+\Delta T$ can be predicted by adding the change in the position of the object, $\Delta x_i(t+\Delta T)$, obtained from equation (3) to the position of the target, $x_i(t)$, at the previous time t.

$$x_i(t+\Delta T) = x_i(t)+\Delta x_i(t+\Delta T) \qquad (7)$$

This is the tracking trajectory $x_i(t)$ of the wall, and it is possible to determine the vibration velocity with high accuracy by repeating this estimation while

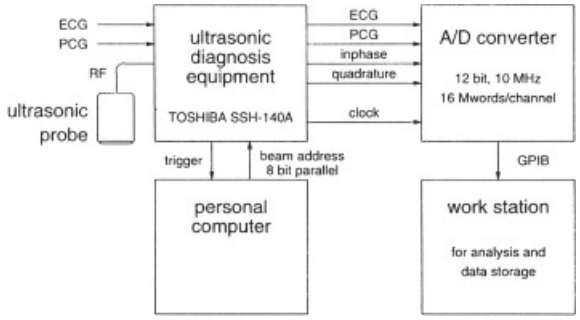

Fig. 1 System for measuring in vivo.

tracking arterial wall motion.

2.3 In vivo measurement system

Fig. 1 shows a schematic diagram of the system used to take measurements in vivo. Ultrasonic pulses are transmitted to several sites arbitrarily selected on the arterial wall from the 7.5 MHz linear US probe of the US diagnostic equipment. A new beam address can be assigned to each pulse by updating 8-bit data.

Ultrasonic pulses reflected by the arterial wall return to the probe, detected by quarature modulation, and are separated into a real part signal $z_{\mathrm{re}}(x_i; t)$, and an imaginary part signal, $z_{\mathrm{im}}(x_i; t)$, and then digitized using a sampling frequency of 10 MHz. Sampled data were transmitted to the workstation through the GPIB cable and analyzed.

The spatial resolution when acquiring data in vivo is in the beam width of the ultrasound beam in the beam focal plane, and recording with conventional US diagnostic equipment at the spatial resolution in M-mode is possible. Minimum measurable vibration velocity is 0.5 mm/s[2)] in the experimental setting. The frequency of detectable vibration depends on the Nyquist frequency of the pulse repetition frequency (PRF) in the two-way US signal. Vibration can be measured at frequencies of up to 3 kHz when the PRF is 6 kHz.

3. Basic experiments with silicone rubber tubes.

3.1 Experimental system with a ventricular assist device (VAD)

Fig. 2 shows a schematic diagram showing the experimental system used here. The silicone rubber tube is placed in a water bath and a pulsatile flow is sent through the silicone rubber tube by the ventricular assist device (VAD). The vibration velocity $v_i(t)$ on the wall of the tube is measured as described in 2.3.

The inner diameter of the silicone rubber tube was 12 mm ; its wall thickness was approximately 1 mm. The elastic modulus (E) was obtained using the following equation, in which an inner radius is R_i and outer radius is R_o, after $\Delta P/\Delta R_o$ was obtained by the least-squared approach using a measured result of the

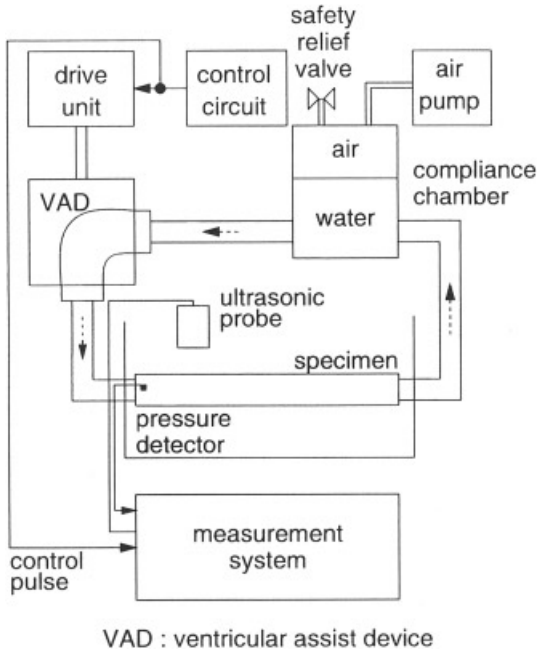

Fig. 2 Experimental system using a ventricular assist device (VAD) to measure vibration signals on the wall of a silicone tube.

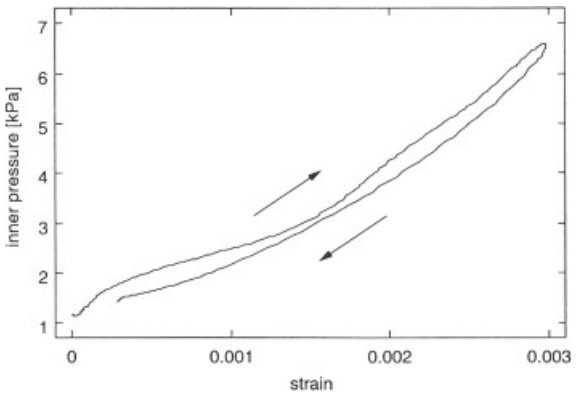

Fig. 3 Experimental results of relationship between applied inner pressure and strain on silicone tube.

increased outer radius ΔR_o when the inner pressure P was changed by ΔP.

$$E = \frac{3}{2}\frac{\Delta P}{\Delta R_o}\frac{R_i^2 R_o}{R_o^2 - R_i^2} \qquad (8)$$

Fig. 3 shows the inner pressure of the silicone rubber tube and the strain on it. Elastic modulus (E) as obtained by Equation (8), was approximately 8 MPa. Using this silicone rubber tube, vibrations on the wall produced by pulsatile flow were measured with and without stenosis in the tube. Stenosis was produced artificially by constricting part of the tube by tying a thread around it. Stenotic rate of the inner radius was 20%, and the liquid in the tube was tap water.

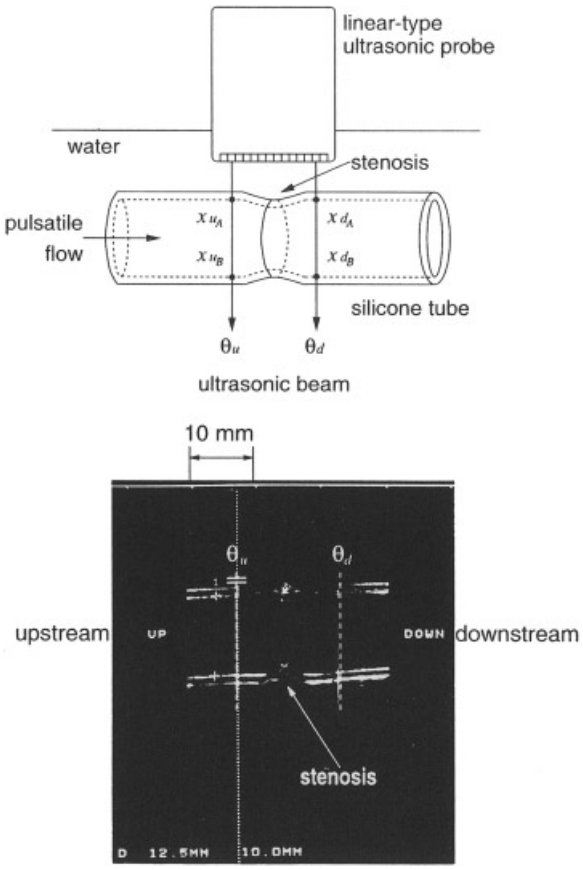

Fig. 4 (a) Measurement points on a silicone tube with stenosis. (b) B-mode image of the silicone tube with stenosis.

Vibration velocity was measured almost simultaneously at four points on the wall : two points on the anterior wall and two points on the posterior wall approximately 7.5 mm upstream θ_u and downstream θ_d of the stenosis. The PRF of ultrasonic transmission was set at 6 kHz. Ultrasonic transmission was performed reciprocally ($N=2$) at beam positions θ_u and θ_d, and the PRF of ultrasonic transmission in each direction is 3 kHz. **Fig. 4 a** shows measurement points on a silicone rubber tube with stenosis ; and **Fig. 4 b**, B-mode images of the silicone rubber tube with stenosis.

3.2 Measurement of wall vibration on the silicone rubber tube

Fig. 5 (**1**) shows signals driving the ventricular assist device (VAD) (**a**), vibration velocity signals $v(x_{u_A};t)$ on the anterior wall at an upstream site of the stenosis θ_u (**b**), vibration velocity signals $v(x_{u_B};t)$ on the posterior wall at an upstream site of the stenosis, velocity signals of changes in the inner diameter $\Delta v(x_u;t) = v(x_{u_A};t) - v(x_{u_B};t)$ (**d**), and signals of changes in the inner diameter $\Delta d(x_u;t) = \int_0^t \Delta v(x_u;t)dt$. The FFT Doppler spectrum of blood flow from upstream to downstream obtained using a conventional US system (**f**) is also shown.

Fig. 5 (**2**) also shows vibration velocity signals $v(x_{d_A};t)$, $v(x_{d_B};t)$ on the anterior and posterior walls downstream $\Delta\theta_d$, velocity signals of changes in the inner diameter $\Delta v(x_d;t)$, and signals of changes in the inner diameter $\Delta d(x_d;t)$. **Fig. 6** (**1**) and (**2**) similarly show the measured results of the same parameters using the silicone rubber tube without stenosis upstream θ_u and downstream θ_d. The following can be seen in these figures.

1) When the silicone rubber tube with stenosis is used, it can be seen in **Fig. 5** that high-frequency signals are included at a downstream site, while they are included at an upstream site in vibration velocity signals both at the anterior and posterior walls. Consequently, high-frequency signals are also included in the velocity signals of changes in the inner diameter. These high-frequency signals are not included when the tube is not constricted (**Fig. 6**).

2) Phase of velocity signals of change in the inner diameter reverse upstream and downstream from the stenotic site immediately after VAD-generated pulsatile flow. As a result, changes in the inner diameter also reverse in phase, downstream from the stenosis in particular, and the anterior and posterior walls are displaced toward the decreasing direction of the inner diameter in the pulsatile flow phase. We assume that there was negative pressure downstream.

3) With respect to measurement on a silicone rubber tube with stenosis, **Table 1** shows correlation coefficients ρ of velocity signals of vibration on the anterior wall at upstream and downstream sites $v(x_{u_A};t)$, $v(x_{d_A};t)$, velocity signals of vibration on the posterior wall $v(x_{u_B};t)$, $v(x_{d_B};t)$, velocity signals of changes in the inner diameter $\Delta v(x_u;t)$, $\Delta v(x_d;t)$ and their combinations between the times from immediately after pulsatile outflow $T_0=0$ s and $T_0=0.6$ s. Correlation coefficients ρ can be obtained from the following equation with respect to two velocities $v_i(t)$, and $v_j(t)$.

$$\rho = \frac{\frac{1}{T_0}\int_0^{T_0} v_i(t)v_j(t)dt}{\sqrt{\frac{1}{T_0}\int_0^{T_0} v_i(t)^2dt}\sqrt{\frac{1}{T_0}\int_0^{T_0} v_j(t)^2dt}} \quad (9)$$

When a stenotic condition was created in the tube, the correlations between upstream and downstream from the stenosis decreased on the anterior and posterior walls. It was also seen that the correlation between the anterior and posterior walls was slightly lower downstream from stenosis than upstream. We consider that this resulted from simultaneous movement of the silicone rubber tube and was not the same upstream and downstream from the stenosis. Velocity signals of inner diameter at the downstream and upstream sites were opposite in phase.

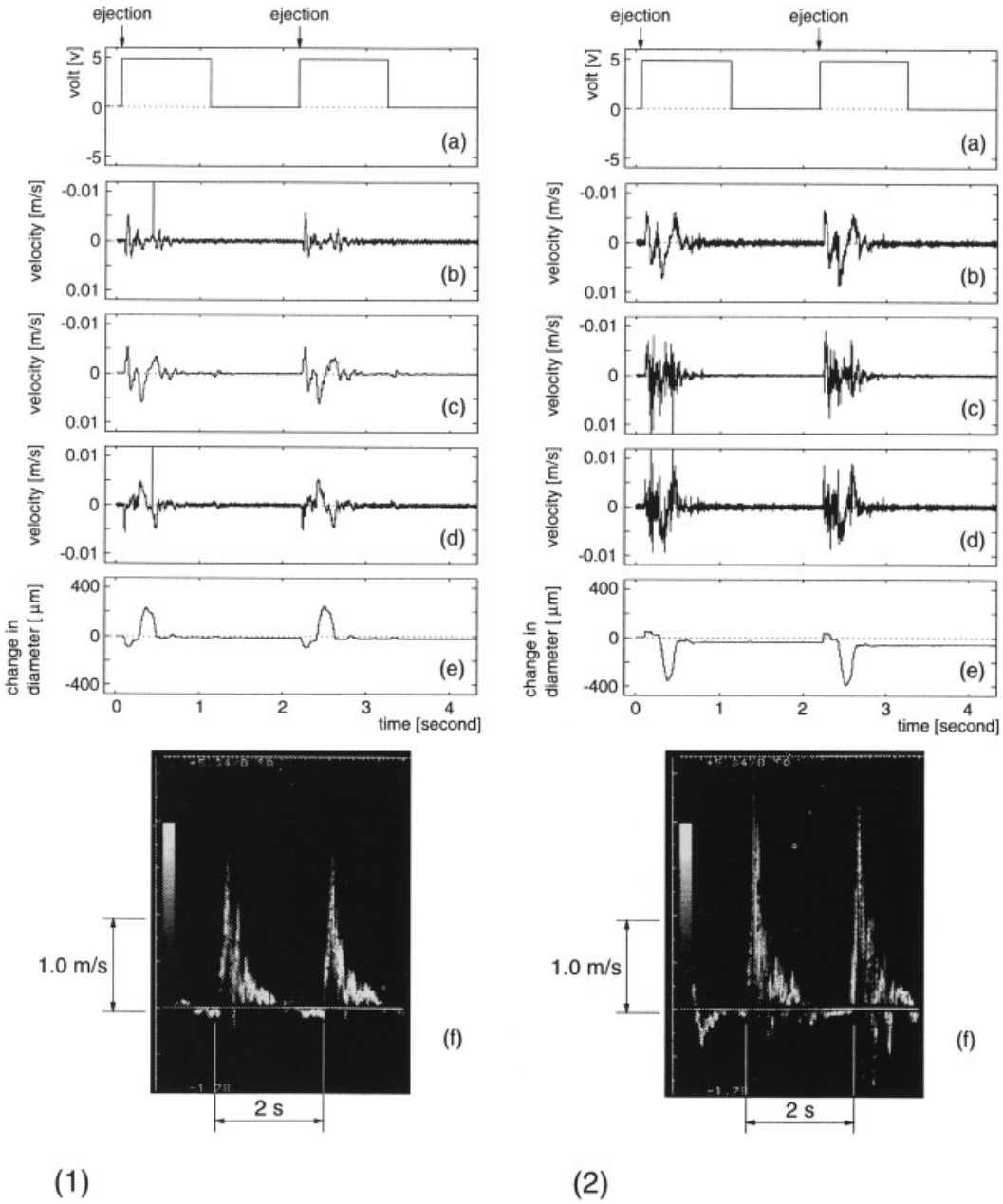

Fig. 5 Experimental results obtained from a silicone tube with stenosis. (1) Measurement point θ_u at an upstream location. (2) Measurement point θ_d at a downstream location. (a) Signal driving the ventricular assist device (VAD). (b) Small vibration signals $v(x_{u_A};t)$ and $v(x_{d_A};t)$ on the anterior wall. (c) Small vibration signals $v(x_{u_B};t)$ and $v(x_{d_B};t)$ on the posterior wall. (d) Velocity signals $\Delta v(x_u;t)$ and $\Delta v(x_d;t)$ of inner diameter. (e) Change in inner diameter $\Delta v(x_u;t)$ and $\Delta v(x_d;t)$. (f) FFT Doppler spectrum of blood flow obtained using ultrasonic diagnostic equipment.

Table 1 Correlation coefficients of small vibration signals measured on a silicone tube with stenosis

Small vibration signals on the anterior wall	Upstream	$v(x_{u_A};t)$	$\leftrightarrow$	Downstream	$v(x_{d_A};t)$	0.489
Small vibration signals on the posterior wall	Upstream	$v(x_{u_B};t)$	$\leftrightarrow$	Downstream	$v(x_{d_B};t)$	0.489
Velocity signals of inner diameter	Upstream	$\Delta v(x_u;t)$	$\leftrightarrow$	Downstream	$\Delta v(x_d;t)$	-0.714
Upstream wall vibration signals	Anterior wall	$v(x_{u_A};t)$	$\leftrightarrow$	Posterior wall	$v(x_{u_B};t)$	0.547
Downstream wall vibration signals	Anterior wall	$v(x_{d_A};t)$	$\leftrightarrow$	Posterior wall	$v(x_{d_B};t)$	0.442

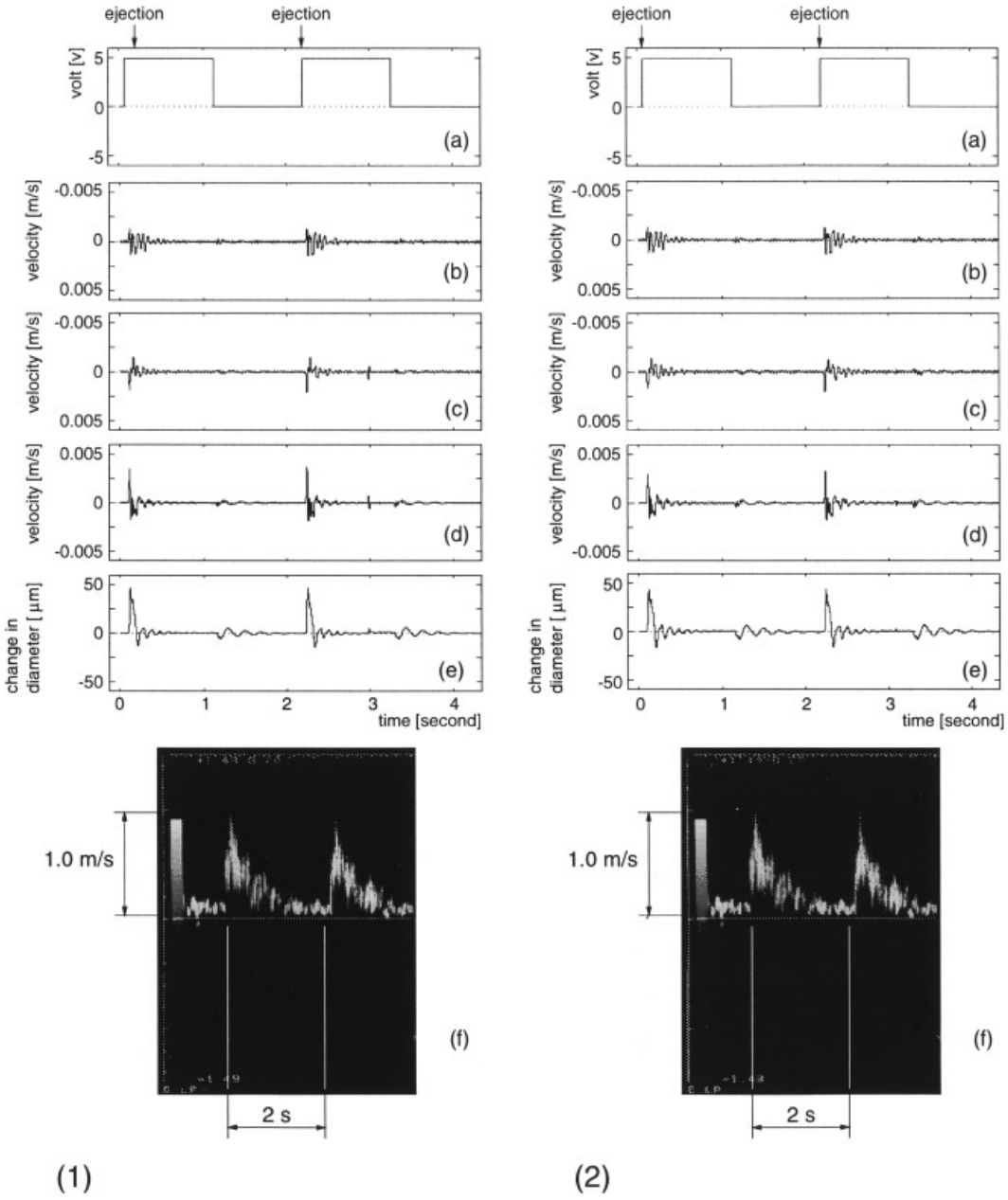

Fig. 6 Experimental results obtained from a silicone tube without stenosis. (1) Measurement point θ_u at an upstream location. (2) Measurement point θ_d at a downstream location. (a) Signal driving the ventricular assist device (VAD). (b) Small vibration signals $v(x_{u_A}; t)$ and $v(x_{d_A}; t)$ on the anterior wall. (c) Small vibration signals $v(x_{u_B}; t)$ and $v(x_{d_B}; t)$ on the posterior wall. (d) Velocity signals $\Delta v(x_u; t)$ and $\Delta v(x_d; t)$ of inner diameter. (e) Change in inner diameter $\Delta v(x_u; t)$ and $\Delta d(x_2; t)$. (f) FFT Doppler spectrum of blood flow obtained using ultrasonic diagnostic equipment.

Table 2 Correlation coefficients of small vibration signals measured on a silicone tube with stenosis

Small vibration signals on the anterior wall	Upstream	$v(x_{u_A}; t)$	$\leftrightarrow$	Downstream	$v(x_{d_A}; t)$	0.963
Small vibration signals on the posterior wall	Upstream	$v(x_{u_B}; t)$	$\leftrightarrow$	Downstream	$v(x_{d_B}; t)$	0.967
Velocity signals of inner diameter	Upstream	$\Delta v(x_u; t)$	$\leftrightarrow$	Downstream	$\Delta v(x_d; t)$	0.980
Upstream wall vibration signals	Anterior wall	$v(x_{u_A}; t)$	$\leftrightarrow$	Posterior wall	$v(x_{u_B}; t)$	−0.079
Downstream wall vibration signals	Anterior wall	$v(x_{d_A}; t)$	$\leftrightarrow$	Posterior wall	$v(x_{d_B}; t)$	0.142

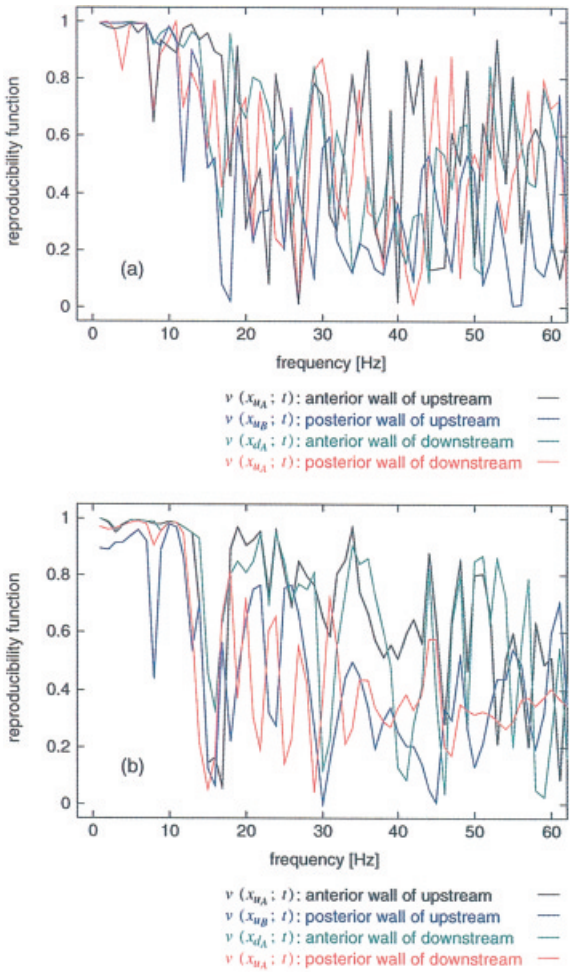

Fig. 7 Reproducibility function of small vibration signals from the wall of the silicone tube. (a) Silicone tube with stenosis. (b) Silicone tube without stenosis.

4) **Table 2**, on the other hand, shows correlation coefficients ρ of velocity signals of vibration on the anterior wall of upstream and downstream sites $v(x_{u_A};t)$, $v(x_{d_A};t)$, velocity signals of vibration on the posterior wall $v(x_{u_B};t)$, $v(x_{d_B};t)$, and velocity signals of changes in the inner diameter $\Delta v(x_u;t)$, $\Delta v(x_d;t)$ between the times from immediately after pulsatile outflow $T_0=0$ s and $T_0=0.6$ s. When stenosis was not placed in the tube, the correlation of velocity signals of the inner diameter was higher at both the upstream and downstream sites and between the anterior and posterior walls. Correlation between velocity signals of the inner diameter was lower between the anterior and posterior walls $v(x_{u_A};t)\leftrightarrow v(x_{u_B};t)$ of the upstream site than between the anterior and posterior walls $v(x_{d_A};t)\leftrightarrow v(x_{d_B};t)$ of the downstream site, however, probably because of a subtle difference in axial tension between the anterior and posterior walls that affected the vibration velocity signals when the silicone rubber tube was fixed in the experiment. We also consider that these effects could diminish when the tube was constricted, as a result of the energy of pulsatile outflow mostly converted into static pressure that affects the inner diameter. We thus evaluated reproducibility of vibration velocity signals at the anterior and posterior walls in the frequency area, using the reproducibility function[13]. The reproducibility function $|\hat{r}_0(f)|^2$ can be obtained with the following equation.

$$|\hat{r}_0(f)|^2=\frac{\left|\sum_{i=1}^{M}V_i(f)\right|^2}{M\sum_{i=1}^{M}|V_i(f)|^2} \qquad (10)$$

Where $V_i(f)$ is the spectrum of the velocity of vibration and M is the number of pulses. **Fig. 7** (**a**) shows evaluation results produced by the reproducibility function of vibration velocity signals from the anterior and posterior walls of the silicone rubber tube with stenosis. **Fig. 7** (**b**) shows results obtained when stenosis was not present. Correlation is shown either with or without stenosis, as there is high reproducibility between pulses in the component of frequency that is less than 10 Hz, which is the main component of the VAD pulse signals at the anterior and posterior walls.

5. US Doppler waveform revealed turbulence and back flow downstream from stenosis. We think that changes in blood flow downstream from stenosis strongly influence wall vibration in those sections of the arteries.

4. Measurement of wall vibration on the human carotid artery.

The wall vibration velocity was obtained from the carotid artery, between the common carotid artery and the carotid sinus, of a 40-year-old female patient with arteriosclerosis, and from the carotid artery, between the common carotid artery and the carotid sinus, of a 25-year-old healthy male subject. Measurements were taken at eight locations along the anterior and posterior walls at beam locations θ_1 and θ_2 at the upstream sites, stenosis θ_3, and downstream site θ_4. The PRF was set at 6 kHz. PRF at each measurement point was 1.5 kHz, as measurement was performed at each point in turn ($N=4$). **Fig. 8, 9** show B-mode images showing the points of measurement for the female patient with arteriosclerosis and the 25-year-old healthy male subject, respectively. Atherosclerotic plaque was detected on the posterior wall of the carotid artery in the 40-year-old female patient with arteriostenosis. The measuring function of the US system used to analyze B-mode images showed the inner diameter d_n of the artery to be approximately 8.3 mm; thickness of the plaque, 2.2 mm (the approximate inner diameter at the stenotic site was $d_s=8.3-2.2=6.1$ mm); and the stenotic rate of the inner diameter η, approximately 27%[12], using

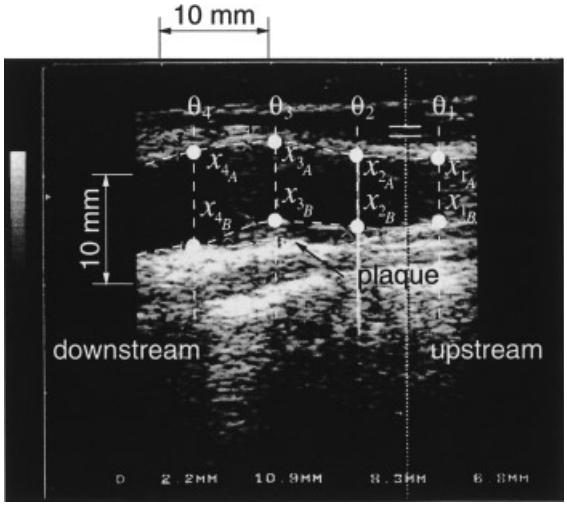

Fig. 8 B-mode image of arteriostenosis lesion of the carotid artery of a 40-year-old female patient with atherosclerosis.

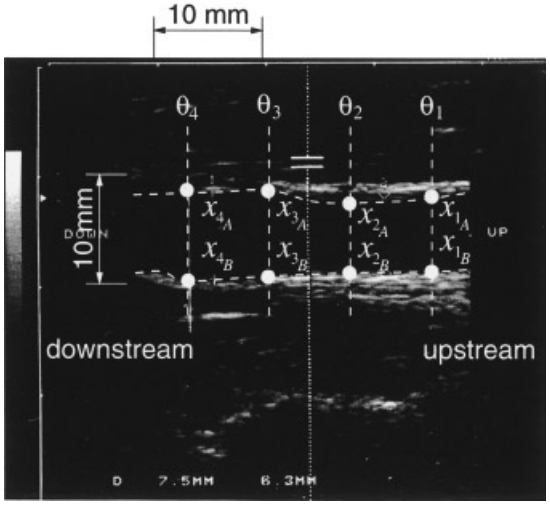

Fig. 9 B-mode image of carotid artery of a 25-year-old healthy male subject.

equation (11).

$$\eta = \frac{d_n - d_s}{d_n} \times 100 \ [\%] \qquad (11)$$

Fig. 10 (**1**) shows the electrocardiograms (**a**) of the 40-year-old female patient with arteriosclerosis, vibration velocity signals $v(x_{1_A}; t)$ (**b**) on the anterior wall x_{1_A} at the beam site θ_1 on the carotid artery (upstream distal side from stenosis), vibration velocity signals $v(x_{1_B}; t)$ (**c**) on the posterior wall x_{1_B}, velocity signals $\Delta v(x_1; t)$ of changes in the inner diameter (**d**), and signals $\Delta d(x_1; t)$ of changes in the inner diameter. Also shown is the FFT Doppler spectrum of blood flow velocity at the point of measurement on the arterial wall (**f**). Similarly, **Fig. 10** (**2**), (**3**), and (**4**) show results obtained from position x_2 at measuring point θ_2 (upstream proximal site from stenosis), measurement results of x_3 at measuring point θ_3 (stenosis), and measurement results of x_4 at measuring point θ_4 (downstream).

Also, **Fig. 11** (**1**), (**2**), (**3**), and (**4**) show results at four points of measurement at upstream and downstream sites on the carotid artery, between the common carotid artery and carotid sinus in the 25-year-old healthy male subject.

These results would appear to justify the following conclusions.

1) Vibration velocity signals from $v(x_{1_A}; t)$ to $v(x_{4_A}; t)$ on the anterior wall of the carotid artery of the 40-year-old female patient with arteriosclerosis show no major change upstream from the stenosis, although it is clear that the high-frequency components are included markedly. Further, vibration velocity signals from $v(x_{1_B}; t)$ to $v(x_{4_B}; t)$ show that the high-frequency components are included between the upstream and downstream sites.

2) The amplitude of the high-frequency components increases downstream from stenosis, with respect to velocity signals from $\Delta v(x_1; t)$ to $\Delta v(x_4; t)$ of the change in the inner diameter obtained from the difference of vibration velocity between the anterior and posterior walls as shown in **Fig. 10**. Although upstream signal amplitude does not change markedly, it decreases suddenly immediately after reaching the downstream stenotic site. Changes in the inner diameter were therefore smaller at the downstream site than at the upstream site, probably because static pressure (blood pressure) decreases and dynamic pressure increases when blood flow passes through a stenotic site, and because static pressure takes longer to recover at the downstream from stenosis than at the upstream site, and blood flow becomes turbulent because of sudden channel dilation. FFT Doppler spectra of blood-flow velocity measured by the US system ate thought to behave similarly, because peak blood-flow velocity at the downstream site immediately after the stenosis changes less than at the stenosis. Turbulent flow and back flow appear downstream from stenosis, and it would appear that flow changes caused by the stenosis markedly affect vibration of the wall, particularly at the downstream site. In addition, back flow appears upstream from the stenosis, probably because of stenotic changes upstream of the point of measurement. The high-frequency components included in the vibration velocity signals on the upstream wall have now been confirmed.

3) **Table 3** shows correlation coefficients ρ of vibration velocity signals measured between vibration velocity signals from $v(x_{1_A}; t)$ through $v(x_{4_A}; t)$ of the anterior wall, vibration velocity signals measured between vibration velocity signals from $v(x_{1_B}; t)$ through $v(x_{4_B}; t)$ of the posterior wall, and velocity

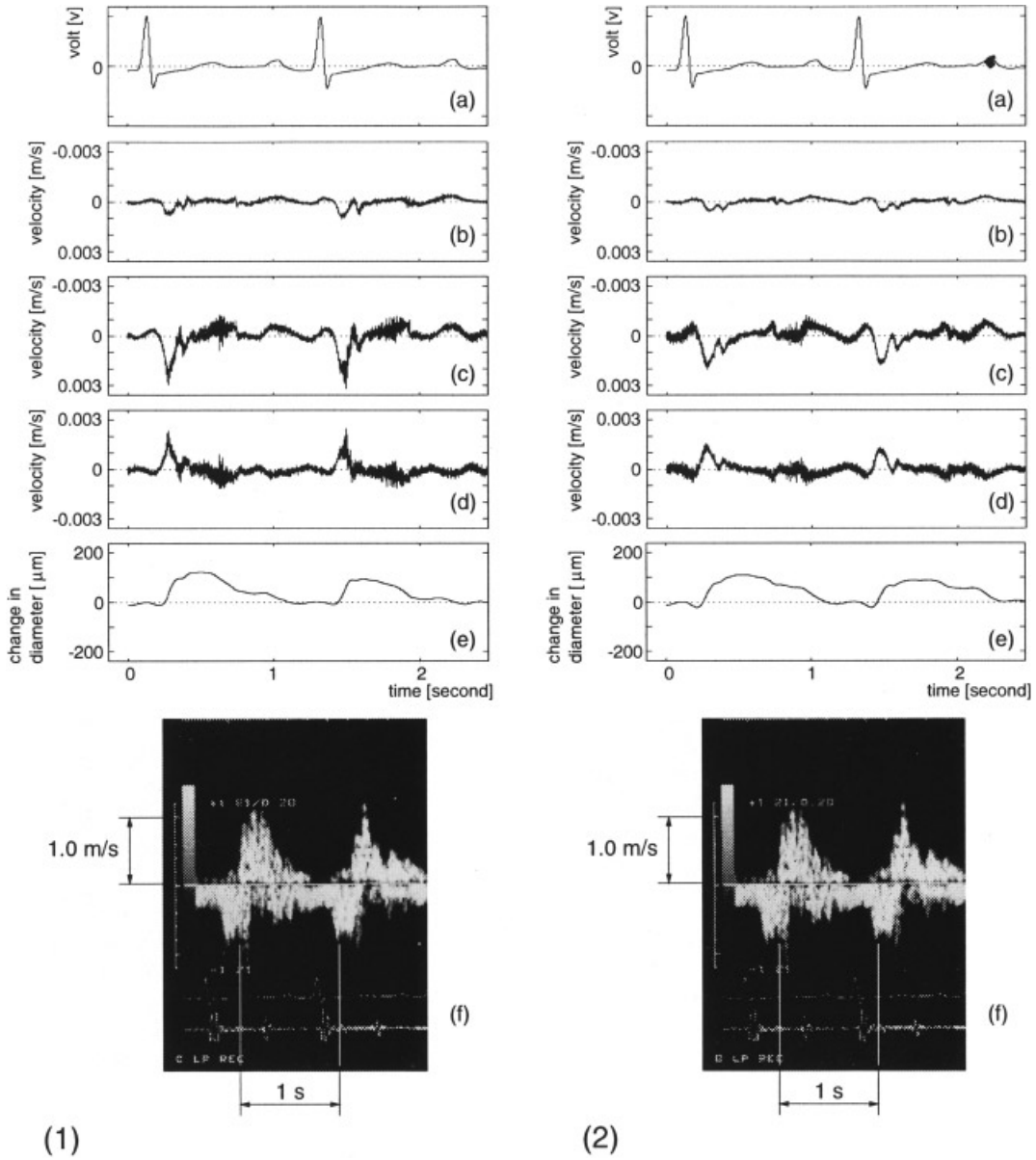

Fig. 10 In vivo experimental results obtained from the carotid artery of the patient with atherosclerosis shown in Fig. 8. (1) Measurement point θ_1. (2) Measurement point θ_2. (a) ECG signal. (b) Small vibration signals $v(x_{1_A}; t)$ and $v(x_{2_A}; t)$ on the anterior wall. (c) Small vibration signals $v(x_{1_B}; t)$ and $v(x_{2_B}; t)$ on the posterior wall. (d) Velocity signals of $\Delta v(x_1; t)$ and $\Delta v(x_2; t)$ of inner diameter. (e) Change in inner diameter $\Delta d(x_1; t)$ and $\Delta d(x_2; t)$. (f) FFT Doppler spectrum of blood flow obtained using ultrasonic diagnostic equipment. (3) Measurement point θ_3. (4) Measurement point θ_4. (a) ECG signal. (b) Small vibration signals $v(x_{3_A}; t)$ and $v(x_{4_A}; t)$ on the anterior wall. (c) Small vibration signals $v(x_{3_B}; t)$ and $v(x_{4_B}; t)$ on the posterior wall. (d) Velocity signals of $\Delta v(x_3; t)$ and $\Delta v(x_4; t)$ of inner diameter. (e) Change in inner diameter $\Delta d(x_3; t)$ and $\Delta d(x_4; t)$. (f) FFT Doppler spectrum of blood flow obtained using ultrasonic diagnostic equipment.

showing changes in the inner diameter from $\Delta v(x_1; t)$ through $\Delta v(x_4; t)$ at beam positions θ_1 to θ_4. The correlation of signals is lower both on the anterior and posterior walls between the upstream θ_2 and the downstream θ_4. Correlation between the anterior and posterior walls is lower at downstream location θ_4 than at the upstream location θ_2. These results appear to support the view that turbulence resulting from stenosis affects vibrations on the arterial wall.

4) **Table 4**, on the other hand, shows correlation cofficients ρ between vibration velocity signals from

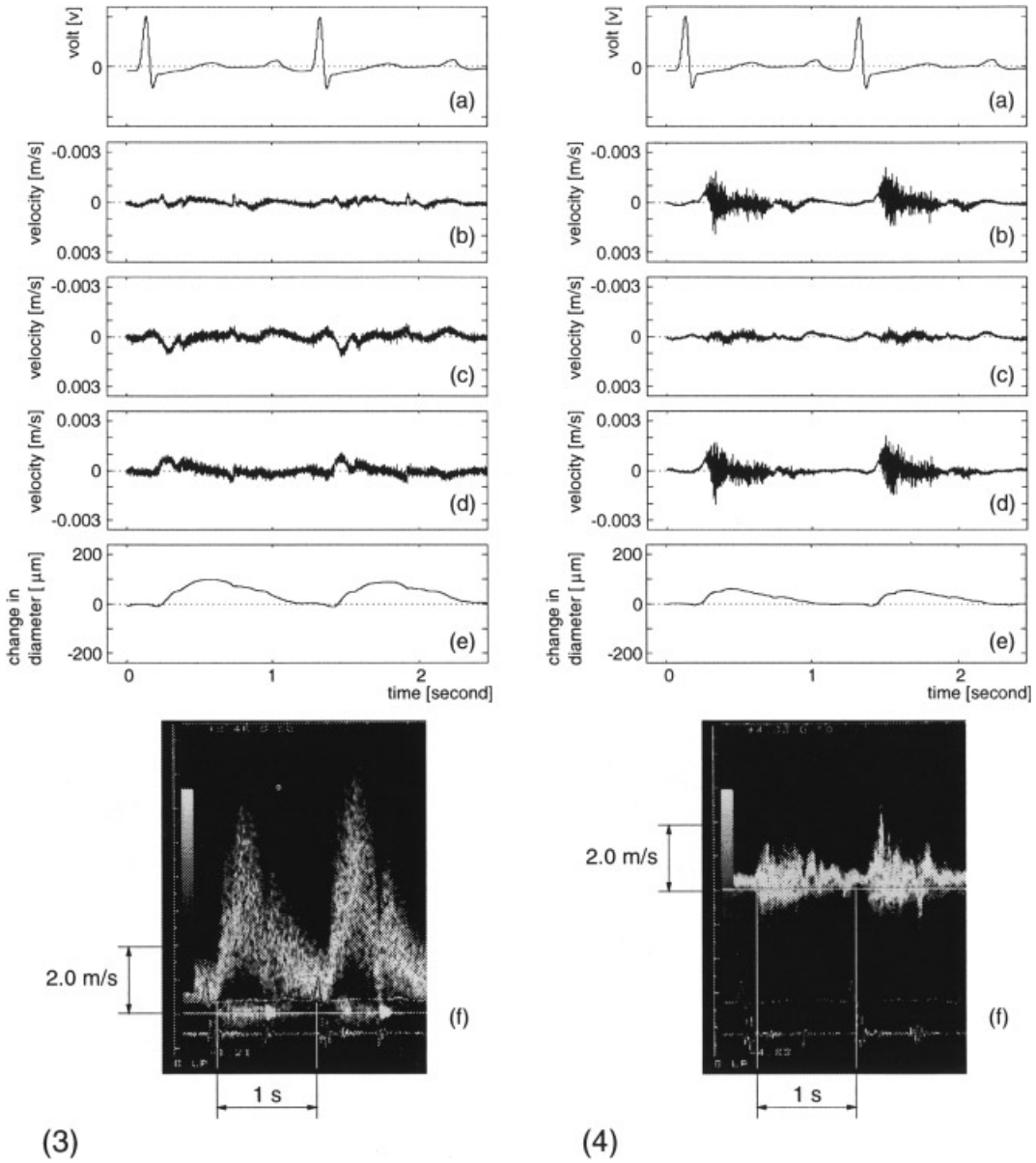

Fig. 10 In vivo experimental results obtained from the carotid artery of the patient with atherosclerosis shown in Fig. 8. (1) Measurement point θ_1. (2) Measurement point θ_2. (a) ECG signal. (b) Small vibration signals $v(x_{1_A};t)$ and $v(x_{2_A};t)$ on the anterior wall. (c) Small vibration signals $v(x_{1_B};t)$ and $v(x_{2_B};t)$ on the posterior wall. (d) Velocity signals of $\Delta v(x_1;t)$ and $\Delta v(x_2;t)$ of inner diameter. (e) Change in inner diameter $\Delta d(x_1;t)$ and $\Delta d(x_2;t)$. (f) FFT Doppler spectrum of blood flow obtained using ultrasonic diagnostic equipment. (3) Measurement point θ_3. (4) Measurement point θ_4. (a) ECG signal. (b) Small vibration signals $v(x_{3_A};t)$ and $v(x_{4_A};t)$ on the anterior wall. (c) Small vibration signals $v(x_{3_B};t)$ and $v(x_{4_B};t)$ on the posterior wall. (d) Velocity signals of $\Delta v(x_3;t)$ and $\Delta v(x_4;t)$ of inner diameter. (e) Change in inner diameter $\Delta d(x_3;t)$ and $\Delta d(x_4;t)$. (f) FFT Doppler spectrum of blood flow obtained using ultrasonic diagnostic equipment.

$v(x_{1_A};t)$ through $v(x_{4_A};t)$ on the anterior wall, and vibration velocity signals from $v(x_{1_B};t)$ through $v(x_{4_B};t)$ on the posterior wall, and velocity of changes in the inner diameter from $\Delta v(x_1;t)$ through $\Delta v(x_4;t)$ at the measurement positions from θ_1 through θ_4 between $T_0=0$ s and $T_0=0.5$ s, immediately after pulsatile flow at the carotid artery of the 25-year-old healthy male subject. In the carotid artery of this subject, there was a high correlation in the waveforms of the vibration both on the anterior and posterior walls from the upstream to the downstream locations.

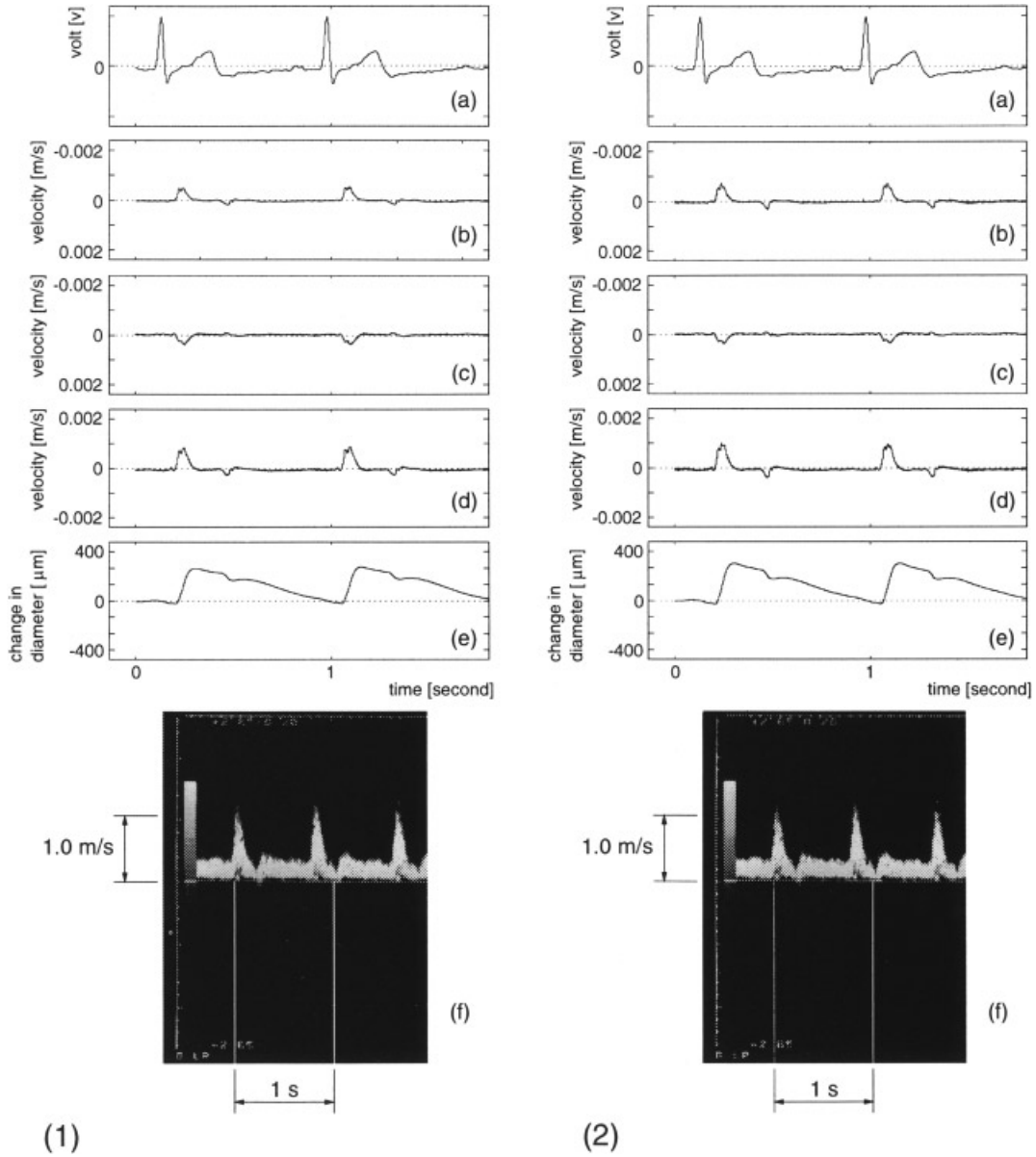

Fig. 11 In vivo experimental results obtained from the carotid artery of the healthy subject in Fig. 9. (1) Measurement point θ_1. (2) Measurement point θ_2. (a) ECG signal. (b) Small vibration signals $v(x_{1_A}; t)$ and $v(x_{2_A}; t)$ on the anterior wall. (c) Small vibration signals $v(x_{1_B}; t)$ and $v(x_{2_B}; t)$ on the posterior wall. (d) Velocity signals $\Delta v(x_1; t)$ and $\Delta v(x_2; t)$ of inner diameter. (e) Change in inner diameter $\Delta d(x_1; t)$ and $\Delta d(x_2; t)$. (f) FFT Doppler spectrum of blood flow obtained using ultrasonic diagnostic equipment. (3) Measurement point θ_3. (4) Measurement point θ_4. (a) ECG signal. (b) Small vibration signals $v(x_{3_A}; t)$ and $v(x_{4_A}; t)$ on the anterior wall. (c) Small vibration signals $v(x_{3_B}; t)$ and $v(x_{4_B}; t)$ on the posterior wall. (d) Velocity signals $\Delta v(x_3; t)$ and $\Delta v(x_4; t)$ of inner diameter. (e) Change in inner diameter $\Delta d(x_3; t)$ and $\Delta d(x_4; t)$. (f) FFT Doppler spectrum of blood flow obtained using ultrasonic diagnostic equipment.

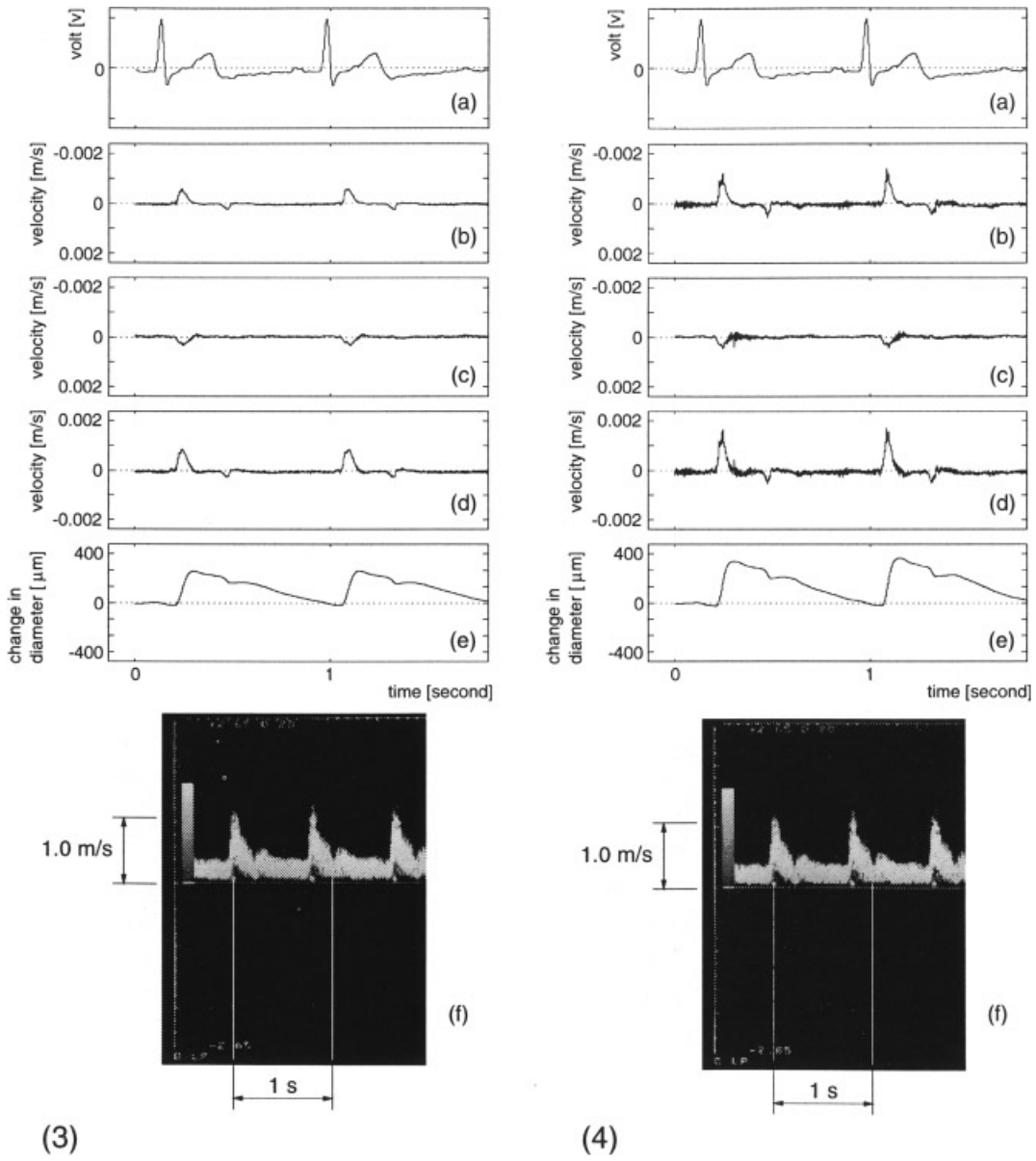

Fig. 11 In vivo experimental results obtained from the carotid artery of the healthy subject in Fig. 9. (1) Measurement point θ_1. (2) Measurement point θ_2. (a) ECG signal. (b) Small vibration signals $v(x_{1_A}; t)$ and $v(x_{2_A}; t)$ on the anterior wall. (c) Small vibration signals $v(x_{1_B}; t)$ and $v(x_{2_B}; t)$ on the posterior wall. (d) Velocity signals $\Delta v(x_1; t)$ and $\Delta v(x_2; t)$ of inner diameter. (e) Change in inner diameter $\Delta d(x_1; t)$ and $\Delta d(x_2; t)$. (f) FFT Doppler spectrum of blood flow obtained using ultrasonic diagnostic equipment. (3) Measurement point θ_3. (4) Measurement point θ_4. (a) ECG signal. (b) Small vibration signals $v(x_{3_A}; t)$ and $v(x_{4_A}; t)$ on the anterior wall. (c) Small vibration signals $v(x_{3_B}; t)$ and $v(x_{4_B}; t)$ on the posterior wall. (d) Velocity signals $\Delta v(x_3; t)$ and $\Delta v(x_4; t)$ of inner diameter. (e) Change in inner diameter $\Delta d(x_3; t)$ and $\Delta d(x_4; t)$. (f) FFT Doppler spectrum of blood flow obtained using ultrasonic diagnostic equipment.

Table 3 Correlation coefficients of small vibration signals measured on the arteriostenosis lesion of the carotid artery of a 40-year-old female patient with atherosclerosis

Small vibration signals on anterior wall		Upstream 1	Upstream 2	Stenotic Portion	Downstream
Upstream 1	$v(x_{1_A};t)$	1.000	0.538	0.369	−0.017
Upstream 2	$v(x_{2_A};t)$	····	1.000	0.187	−0.178
Stenotic portion	$v(x_{3_A};t)$	····	····	1.000	0.391
Downstream	$v(x_{4_A};t)$	····	····	····	1.000
Small vibration signals on posterior wall					
Upstream 1	$v(x_{1_B};t)$	1.000	0.570	0.493	0.255
Upstream 2	$v(x_{2_B};t)$	····	1.000	0.512	−0.051
Stenotic portion	$v(x_{3_B};t)$	····	····	1.000	0.195
Downstream	$v(x_{4_B};t)$	····	····	····	1.000
Velocity signals of inner diameter					
Upstream 1	$\Delta v(x_1;t)$	1.000	0.412	0.372	0.274
Upstream 2	$\Delta v(x_2;t)$	····	1.000	0.438	0.238
Stenotic portion	$\Delta v(x_3;t)$	····	····	1.000	0.242
Downstream	$\Delta v(x_4;t)$	····	····	····	1.000
Vibration signals (Between anterior and posterior walls)					
Upstream 1	$v(x_{1_A};t) \leftrightarrow v(x_{1_B};t)$	0.397	····	····	····
Upstream 2	$v(x_{2_A};t) \leftrightarrow v(x_{2_B};t)$	····	0.539	····	····
Stenotic portion	$v(x_{3_A};t) \leftrightarrow v(x_{3_B};t)$	····	····	0.255	····
Downstream	$v(x_{4_A};t) \leftrightarrow v(x_{4_B};t)$	····	····	····	0.463

Table 4 Correlation coefficients of small vibration signals measured on the carotid artery of a 25-year-old healthy male subject

Small vibration signals on anterior wall		Upstream 1	Upstream 2	Downstream 1	Downstream 2
Upstream 1	$v(x_{1_A};t)$	1.000	0.984	0.970	−0.921
Upstream 2	$v(x_{2_A};t)$	····	1.000	0.984	−0.947
Stenotic portion	$v(x_{3_A};t)$	····	····	1.000	0.960
Downstream	$v(x_{4_A};t)$	····	····	····	1.000
Small vibration signals on posterior wall					
Upstream 1	$v(x_{1_B};t)$	1.000	0.984	0.961	0.869
Upstream 2	$v(x_{2_B};t)$	····	1.000	1.000	0.956
Stenotic portion	$v(x_{3_B};t)$	····	····	1.000	0.865
Downstream	$v(x_{4_B};t)$	····	····	····	0.860
Velocity signals of inner diameter					
Upstream 1	$\Delta v(x_1;t)$	1.000	0.992	0.981	0.944
Upstream 2	$\Delta v(x_2;t)$	····	1.000	0.987	0.952
Stenotic portion	$\Delta v(x_3;t)$	····	····	1.000	0.961
Downstream	$\Delta v(x_4;t)$	····	····	····	1.000
Vibration signals (Between anterior and posterior walls)					
Upstream 1	$v(x_{1_A};t) \leftrightarrow v(x_{1_B};t)$	0.943	····	····	····
Upstream 2	$v(x_{2_A};t) \leftrightarrow v(x_{2_B};t)$	····	−0.956	····	····
Stenotic portion	$v(x_{3_A};t) \leftrightarrow v(x_{3_B};t)$	····	····	−0.907	····
Downstream	$v(x_{4_A};t) \leftrightarrow v(x_{4_B};t)$	····	····	····	−0.854

5. Frequency analysis of velocity signals of change in the inner diameter.

5.1 Power spectrum of velocity signals of change in form by change in the inner diameter

Fig. 12 a, b show the power spectra of velocity signals of change in the inner diameter during the ejection period (from immediately after ejection to $T_0=0.6$ s), with and without stenosis in the silicone rubber tube, respectively. **Fig. 13 a, b** similarly show power spectra of velocity signals of change in the inner diameter during the ejection period (from immediately after ejection to $T_0=0.5$ s) in the carotid arteries of the patient with arteriosclerosis and the healthy subject respectively.

Power spectra from the upstream and downstream locations differ little when there is no stenosis in the silicone rubber tube. When there is stenosis in the tube, however, the power of the high-frequency component increases more downstream than upstream.

Behavior of the carotid artery resembles that of the silicone rubber tube : the power of the high-frequency component increases more at the downstream location than at the upstream location. In the healthy subject, on the other hand, the high-frequency component at the carotid sinus is quite powerful.

We consider that turbulent blood flow at the carotid sinus markedly affects arterial wall vibration in the healthy subject, because there was little difference in S / N of the quadrature modulated US signals (approximately 30 to 40 dB) from the arterial wall.

In the silicone rubber tube, the power of the high-frequency component is large downstream from stenosis. In the carotid artery of the patient with arteriosclerosis, however, the difference disappears in the frequency range of over 250 Hz. This would appear to be related to differences in elasticity : 8 MPa in the silicone rubber tube against several hundred kPa in the human carotid artery, and differences in viscosity in the carotid artery and silicone rubber tube. These differences are also thought to be related to the fact that the power of the high-frequency component of vibration is greater at the upstream location in the silicone rubber tube with stenosis than in the one without stenosis. High-frequency vibration generated by turbulence downstream from stenosis appears to be transmitted to the upstream wall.

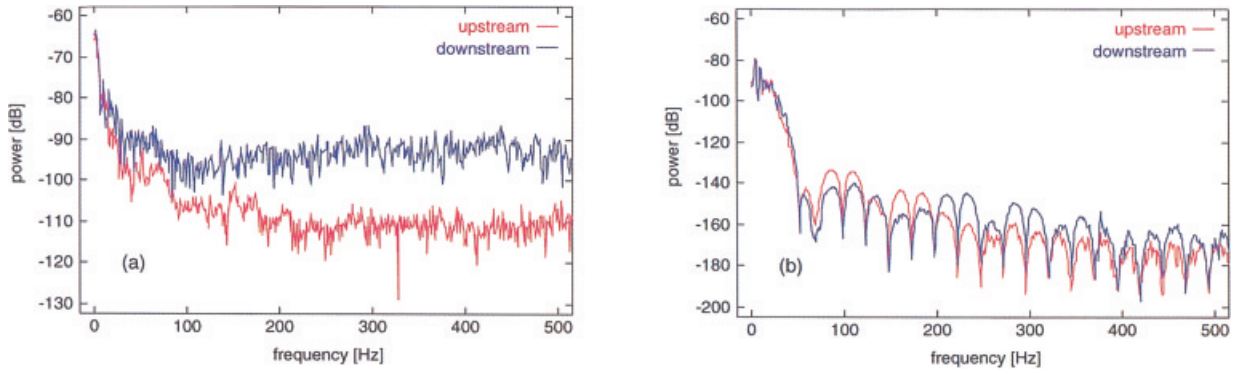

Fig. 12 Power spectra of small vibration signals on the walls of the silicone tube. (a) Silicone tube with stenosis. (b) Silicone tube without stenosis.

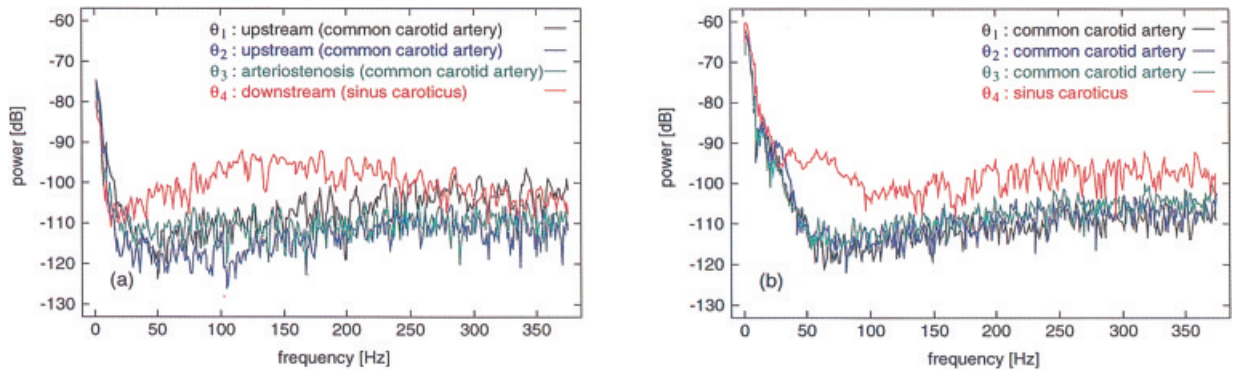

Fig. 13 Power spectra of small vibration signals on the walls at the carotid artery. (a) Patient with atherosclerosis. (b) Healthy subject.

5.2 Evaluation of velocity signals of change in the inner diameter using a reproducibility function

Reproducibility of amplitude and phase of velocity signals of the inner diameter of the silicone rubber tube and the carotid artery is evaluated between pulses. **Fig. 14, 15** show the reproducibility function of both amplitude and phase and of amplitude of velocity signals of the inner diameter alone in silicone rubber tubes with and without stenosis, respectively, during the ejection period (immediately after ejection until $T_0=0.6$ s) in three pulses. **Fig. 16, 17** similarly show reproducibility functions of both amplitude and phase and of amplitude of velocity signals of the inner diameter alone in the carotid artery of the patient with arteriosclerosis and of the healthy subject, respectively, during the ejection period (immediately after ejection until $T_0=0.5$ s).

Reproducibility function for amplitude and phase is obtained from equation (10), as explained in 3.2. Reproducibility function amplitude alone is obtained from the following equation.

$$|\hat{r}_0(f)|^2=\frac{\left(\sum_{i=1}^{M}|V_i(f)|\right)^2}{M\sum_{i=1}^{M}|V_i(f)|^2} \qquad (12)$$

In both the silicone rubber tube with stenosis and the patient with arteriosclerosis, reproducibility of amplitude of velocity signals of the inner diameter downstream from stenosis is high. When amplitude and phase are evaluated at the same time, however, reproducibility between pulses decreases and has frequency components higher than approximately 10 Hz. As shown in **Fig. 12 a, 13 a**, the high-frequency component in the power spectrum between pulses was low in reproducibility. This would appear to be explained by the vibrations with low correlation generated by turbulence being transmitted to the wall.

Furthermore, in the carotid sinus of the healthy subject, reproducibility in frequency components between pulses decreases when it exceeds approximately 10 Hz. In this case also, this low reproducibility between vibrations of low correlation generated by turbulence would appear to be explained by transmission to the arterial wall.

6. Conclusion

We measured vibrations around stenosis in a silicone rubber tube with a constriction and around stenosis in the common carotid artery of a patient with arteriosclerosis, and evaluated the effects of blood flow

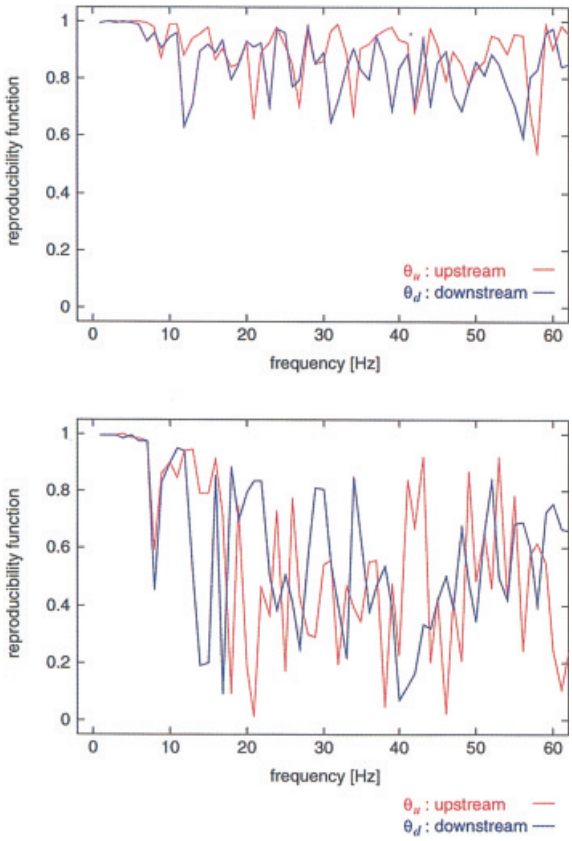

Fig. 14 Reproducibility function of velocity signals of inside diameter of the silicone tube with stenosis. (a) Amplitude. (b) Amplitude and phase.

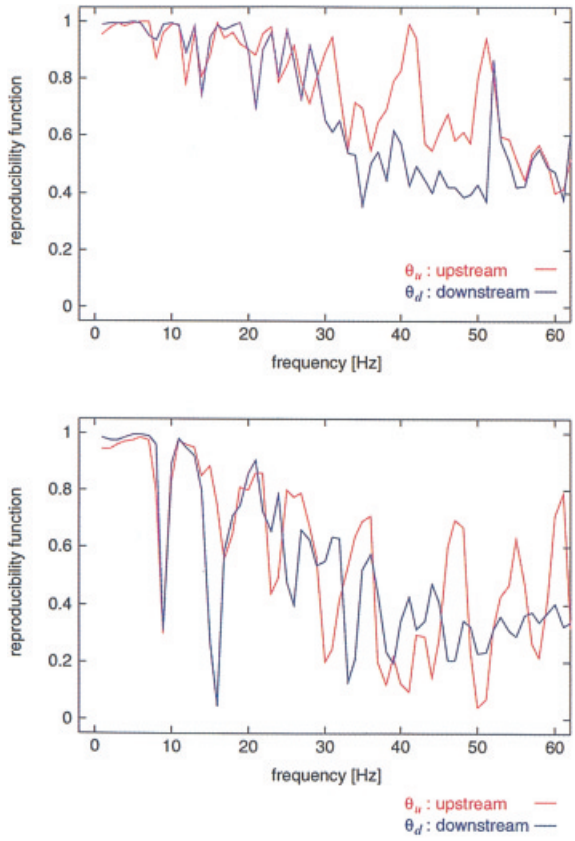

Fig. 15 Reproducibility function of velocity signals of the inside diameter of the silicone tube without stenosis. (a) Amplitude. (b) Amplitude and phase.

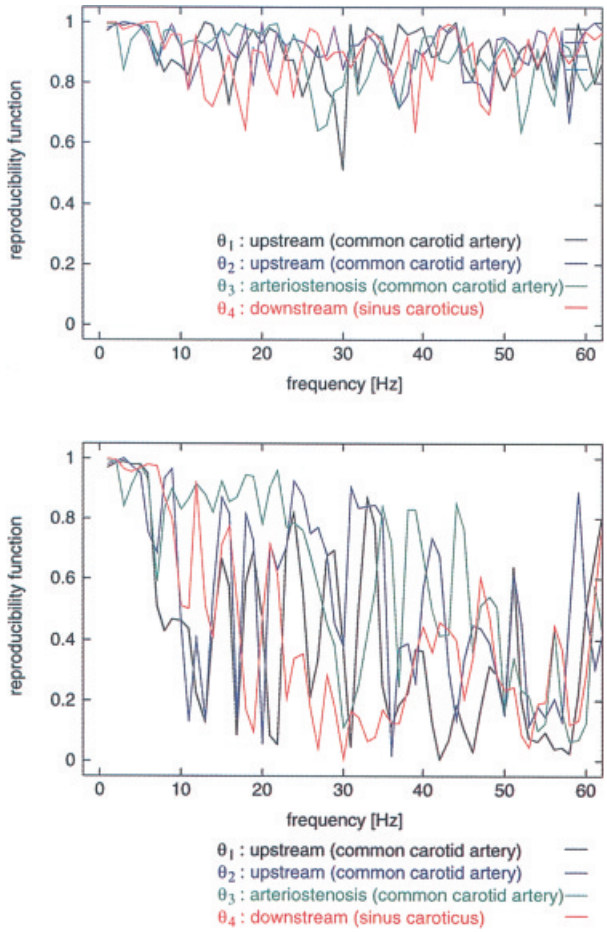

Fig. 16 Reproducibility function of velocity signals of inside diameter of the carotid artery of the patient with atherosclerosis. (a) Amplitude. (b) Amplitude and phase.

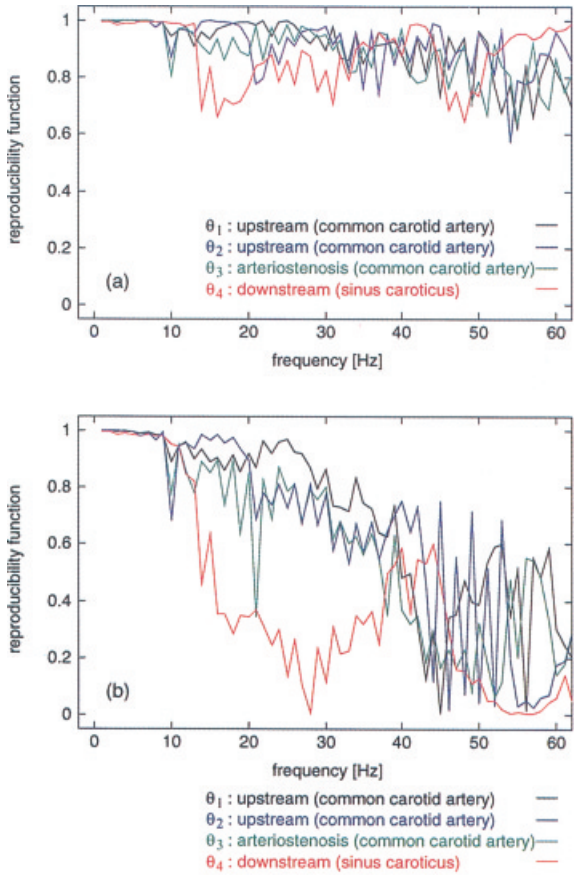

Fig. 17 Reproducibility function of velocity signals of inside diameter of the carotid artery of the healthy subject. (a) Amplitude. (b) Amplitude and phase.

in stenosis on wall vibration. Small vibration of the arterial wall downstream of stenosis differed markedly from that in a healthy subject. With respect to vibration on the arterial wall, the low-frequency component, up to several tens of Hz and caused by the transmission of pressure waves produced by cardiac pulsatile outflow, was recorded. A high-frequency component downstream from stenosis differed from the one described above. The high-frequency component of the vibration observed downstream from stenosis had low reproducibility between pulses. FFT Doppler spectra showed turbulent flow and back flow downstream of stenosis. We therefore presume that changes in blood flow markedly affect wall vibration, particularly downstream from stenosis.

It is thus possible that we can evaluate the effects of pulsatile blood flow on the local arterial wall by measuring and comparing vibrations on the arterial wall. We believe this procedure has potential for estimating the possibility of rupture of atherosclerotic plaques.

References

1) Nonogi H : The Pathorogenesis and treatment of acute coronary syndrome. Recent advances in cardiovascular disease 1998 ; 14 : 100-113. [in Japanese]
2) Hasegawa H, Kanai H, Chubachi N, et al : Evaluation of elastic modulus of the arterial wall by accurate noninvasive measurement of change in thickness of arterial wall. JPN J Med Ultrasonics 1997 ; 24 (6) : 851-860. [in Japanese]
3) Kobayashi T, Ryu H, Yamaguchi T : A computational mechanical analysis of rupture of atheromatous plaque and acute coronary syndrome(ACS). JJME 1998 ; 36 (Suppl) : 441. [in Japanese]
4) Sugawara M : Introduction to Blood Flow : Foundation for Ultrasonic Doppler Measurements. *Tokyo, MS Press,* 1998 : pp. 1-32. [in Japanese]
5) Asaoka N, Matsuoka H: Jpn. J. Clin. Radiol (Supplement) 1998 ; 43(11) : 1396-1402. [in Japanese]
6) Yasaka M, Tutiya T, Yamaguchi T, et al : Ageing and

diseases 1990 ; 3(6) : 893-900. [in Japanese]
7) Kikuchi K, Mekata K, Hasegawa K, et al : On the relationship between blood flow sounds from the cervical carotid artery and cerebrovascular lesions. IEICJ Technical Report 1998 ; EA97-103 (3) : 1-8. [in Japanese]
8) Fukunaka N, Inoue Y, Hasegawa J : Detection system of intracranial blood flow noise for diagnosis of vessel malformation. IEICJ Technical Report 1993 ; EA93-79 (12) : 17-22. [in Japanese]
9) Kanai H, Sato M, Koiwa Y, et al : Transcutaneous measurement and spectrum analysis of heart wall vibrations : *IEEE Trans. on UFFC* 1996 ; 43 : 791-810.
10) Hasegawa H, Kanai H, Hoshimiya N, et al : Measurement of Spatial Distribution of Elasticity of Arterial Wall Using Ultrasound. Reports of the 1999 spring meeting the Acoustical Society of Japan 1999 : 1125-1126. [in Japanese]
11) Antal G. Hudetz : Incremental elastic modules for orthotropic incompressible arteries : *J Biomech* 1979 ; 12 : 651-655.
12) Sano M, Kubota Y, Sumita Y : Medical Technology 1997 ; 25 (5) : 405-427. [in Japanese]
13) Kanai H : Spectrum Analysis of Sound and Vibration. Tokyo, Corona Publishing Co., Ltd., 1999 : pp. 269-271. [in Japanese]